BULLETIN OF THE POLISH ACADEMY OF SCIENCES
TECHNICAL SCIENCES 66, No. 1, 2018
DOI: 10.24425/119063

Specific emitter identification using geometric features of frequency drift curve

Y. ZHAO[1]*, L. WU[1], J. ZHANG[1], and Y. LI[2]

[1]School of Electronics and Information Engineering, Harbin Institute of Technology, Harbin, China
[2]R&D Centre, Chinese Academy of Launch Vehicle Technology, Beijing, China

Abstract. Specific emitter identification (SEI) is a technique for recognizing different emitters of the same type which have the same modulation parameters. Using only the classic modulation parameters for recognition, one cannot distinguish different emitters of a same type. To solve the problem, new features urgently need to be developed for recognition. This paper focuses on the common phenomenon of frequency drift, defines geometric features of frequency drift curve and, finally, proposes a practical algorithm of specific emitter identification using the geometric features. The proposed algorithm consists of three processes: instantaneous frequency estimation based on the adaptive fractional spectrogram, feature extraction of frequency drift curve based on geometric methods for describing a curve and recognition process based on support vector machine. Simulation results show that the identification rate is generally more than 98% above –5 dB of signal to noise ratio (SNR), and real data experiment verifies the practical performance of the proposed algorithm.

Key words: specific emitter identification, geometric features, frequency drift, adaptive fractional spectrogram, support vector machine.

1. Introduction

Specific emitter identification (SEI) is a practical technique applied in both modern electronic warfare and many civilian scenarios [1–3]. In the early identification of radar emitters, researchers primarily focused on the intra-pulse and inter-pulse features, such as the pulse descriptor word (PDW), which can be called intentional modulation characteristics [4, 5]. To avoid being intercepted and recognized, the latest radar emitters are designed with modulation parameters randomly varying [6–8], which brings new serious challenges for emitter identification. Modulation parameters used for recognition can be intentionally changed by the emitter operators, so they are generally classified as intentional modulation features. If only intentional modulation features are used for identification, it is difficult or theoretically impractical to identify more than two emitters of which modulation parameters are changed into the same [9]. SEI is an advanced approach to identify different same-type emitters with the same intentional modulation parameters. SEI is mainly based on some unintentional modulation signatures caused by the physical components embedded in a specific emitter, which the emitter cannot change by itself, such as frequency drift and phase noise [10, 11]. Unfortunately unintentional modulation features used for SEI have not attracted enough attention of researchers.

In specific emitter identification application, once the emitter is activated, the signals sent from the emitter have unique characteristics that can be used to clearly identify the emitter, which can be called "fingerprint" or unintentional modulation features [10, 12, 13]. The causes of unintentional modulation features include amplitude variation, phase noise and frequency drift, in which the features of amplitude variation are usually unstable because of an unknown influence from transmission channel [10–15]. An SEI technique using amplitude features generated by the nonlinearity of the power amplifiers in single-hop and relaying scenarios is presented in [11], and the proposed algorithm is also applicable in fading channels, which makes the work particularly remarkable. Using pulse envelope as the individual feature of an emitter in digital channelized receivers is presented in [15], which is another amplitude-based SEI algorithm. Using the features of phase noise for SEI has also been subject to studies and some good results have been achieved [10, 14]. A comparison of using phase features and frequency features in modulation domain for SEI is discussed in [10]. An SEI algorithm using radio frequency features extracted from time-frequency-energy distribution based on Hilbert-Huang transform is proposed in [12]. A new feature group developed from PDW features based on regression analysis is presented in [13] and the performance of the proposed SEI algorithm is impressive. All the methods mentioned above are mainly traditional time-domain or frequency-domain methods.

Nonlinear dynamics of RF power amplifiers and oscillators can produce nonlinear dynamics characteristics. SEI methods based on nonlinear dynamics features are proposed in [16, 17] and the results show that the proposed SEI algorithms are practical. A fractal method using an improved fractal filter for signal filtering and fractal dimension for identification is proposed in [16]. An SEI algorithm using normalized permutation entropy is presented in [17]. Another nonlinear dynamics method using fractal features constructed by iterated function system (IFS) from basic radar signal parameters is proposed in [18].

*e-mail: yaqinzhao@hit.edu.cn

Manuscript submitted 2016-10-23, revised 2017-02-23, initially accepted for publication 2017-04-12, published in February 2018.

The methods mentioned above are mainly nonlinear dynamics methods.

A fast-decision identification algorithm method for SEI is proposed in [19], playing an important role in expert databases. A hybrid fusion method for specific radar emitter identification based on the kernel canonical correlation analysis (KCCA) and the ambiguity function (AF) description is proposed in [20]. An SEI algorithm using graphical representation of the distribution of radar signal parameters is proposed in [9]. Using the slice of a quadratic time-frequency distribution as the recognition features for SEI is presented in [21] and using the cumulants of the intercepted signal for SEI is presented by [22]. The methods mentioned above are mainly database-based or statistics methods.

In the research area of SEI, Kawalec and Dudczyk are known as authors of numerous works [4, 9, 13, 18, 19]. Their work on SEI can date back to 2004, and it is a continuation of the pioneer studies on emitter recognition of Kawalec before 2004. Their subsequent SEI research mainly develops new methods fully using the abundant traditional pulse parameters results, which makes the whole work remarkable.

SEI aims at finding a specific view and representation of emitters, and there are different views of emitters in different domains, such as the time domain. A schematic timing diagram of a receiver and an emitter is shown in Fig. 1. There are three time length levels in a receiver working process, which are pulse level, slice level and observing time window (OTW) level. An observing time window consists of many compact time slices and generally costs tens of minutes. During a time slice, the receiver receives several pulses of the emitting signal. The period of the time slice is usually several seconds and its width is less than one second. Most of the references mentioned above mainly focus on inter-pulse or intra-pulse information [4, 5, 9, 13, 17, 18, 20, 22, 23], which pertain to pulse level, not long enough in the time dimension. The features used for classification are generally extracted from several continuous pulses. So most of the methods mentioned above are relatively microcosmic and continuous in the time dimension.

There is a phenomenon of frequency drift occurring in an emitter start-up process, mainly caused by temperature increasing, and the warming up procedure usually takes tens of minutes. The frequency drift, mainly from the local oscillator of the emitter, makes the instant carrier frequency of the emitted signals vary in a range depending on the temperature before temperature stabilization. So the frequency drift curve should be fluctuating first, and the fluctuating range decreases as the temperature increases, but the frequency drift curve will fluctuate in a small range when the temperature is finally stable.

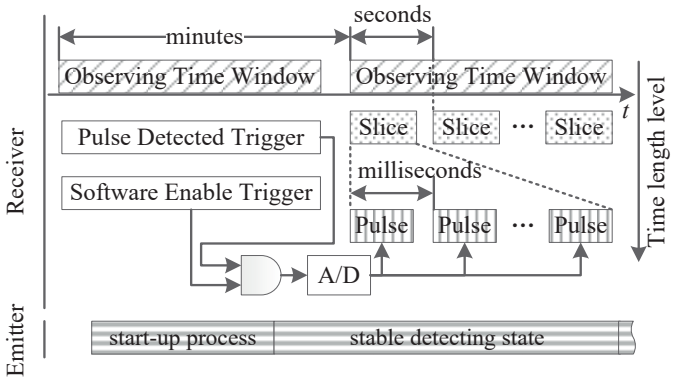

Fig. 1. The schematic timing diagram of a receiver and an emitter

This paper studies specific emitter identification using the unintentional modulation characteristics of frequency drift during the emitter start-up process. The proposed SEI algorithm is usually applied in an ELINT system, which always keeps receiving the electronic signals in a long continuous period, so assuming that the start-up process can be covered completely is reasonable. The proposed algorithm corresponds to the slice level shown in Fig. 1, which is a novel view of electronic emitters, and apparently it is relatively macroscopic and intermittent in the time dimension as compared with the methods mentioned before. The proposed algorithm mainly defines a group of geometric features of the frequency drift curve, which can represent individual geometric differences. At the same time, this paper proves that the extracted features are stable and practical for emitter recognition.

This paper is organized as follows: signal modeling modulated with unintentional modulation characteristics of frequency drift is presented in Section 2; the proposed algorithm for feature extraction from frequency drift curve obtained by the adaptive fractional spectrogram method is presented in Section 3; simulation results and the analysis are presented in Section 4; Section 5 summarizes simulation results and includes the conclusions.

2. Signal modeling

To establish the signal model, the principle behind the unintentional modulation of frequency drift is reviewed and analyzed. The common phenomenon of frequency drift is mainly caused by the instability of an emitter due to the temperature changes and the current changes along with power increasing, which leads to a working frequency deviating from the required frequency [24]. Generally speaking, temperature affects the frequency drift mostly, so this paper mainly focuses on frequency drift along with temperature varying.

Based on experimental results, frequency drift models of three different emitters for simulation with temperature changing are shown in Fig. 2(a). Assuming that the temperature of the three emitters varies from 25°C to 65°C when they are started up from a standby state to a detecting state, the temperature varying rate is different because of a different start-up power. A higher power start-up (HPS) takes 10 minutes and another lower power start-up (LPS) takes 12 minutes before the temperature increasing procedure is finished. Assuming that the energy of emitter is gradually linearly increasing and the energy dissipation power is approximately constant, the temperature is proportional to the time in a certain range until the working heat power equals the energy dissipation to make the temperature static, which is called a stable detecting state. In fact, the assumption of the relationship between temperature and time

does not matter much, which will be explained in the following part. Over a period of start-up time, temperature increases to 65 centigrade, assuming that then the emitter will work stably, heat generating and radiating will be balanced, the temperature will keep constant as shown in Fig. 2(b). The two polylines with different colors in Fig. 2(b) represent different trends of temperature changing over time of the same type emitter operating with two different powers. The higher the power is, the faster the temperature will change to reach a steady operation state and then keep stable during the normal working state.

Frequency drifts over time of three emitters of the same type, working with two different powers, are shown in Fig. 2(c), obtained from the relationship among temperature, time and frequency drift in Fig. 2(a) and Fig. 2(b). Fig. 2 shows that the greater the power is, the more rapidly the frequency shift changes, when the emitter works normally, the frequency shift is gradually being stable.

In practical application, it is unpractical to measure the temperature of emitters. What a receiver can obtain is the relationship between frequency drift and time as shown as Fig. 2(c). The frequency drift curves stretch in t dimension along with the different start-up power condition, which can be called a t-flexibility property and is a challenge for emitter identification. So the specific feature extraction and classification method should be insensitive to the t-flexibility changes made by a different start-up power and classify the emitter frequency drift curves with different powers of the same emitter into the same class, which can be called anti-t-flexibility ability.

The assumption of the relationship between temperature and time is for the convenience of analysis. Nonlinear correlation can be piecewise approximation by linear functions with different piecewise slope. The proposed SEI algorithm can extract the features without measurement the temperature because of the anti-t-flexibility ability, which means the relationship between temperature and time does not affect the specific feature extraction and classification as long as the temperature keeps increasing during the start-up process.

Generally speaking, it takes tens of minutes to increase the temperature and more time to cool the emitters down, so it takes hours to finish a complete measurement period of a start-up process. Considering that it takes too much time to get enough samples, and the experiment conditions, such as SNR, are not easy to be set in real-data measurement, so for algorithm development, this paper builds six frequency drift models of three different emitters with two different start-up powers based on experimental results, as shown in Fig. 2(c). The simulations in the following parts of this paper are theoretical, but all the parameters are based on real signal sources measurement results, and the real data verification experiment will prove the practical performance of the proposed algorithm.

The signal source $s_{fd}(t)$ modulated from pure signal $s(t)$ with the frequency shift f_d can be expressed as

$$s_{fd}(t) = s(t) \times \exp(j2\pi f_d t). \tag{1}$$

The frequency drift curve is abbreviated to FD-curve in the subsequent parts of this paper.

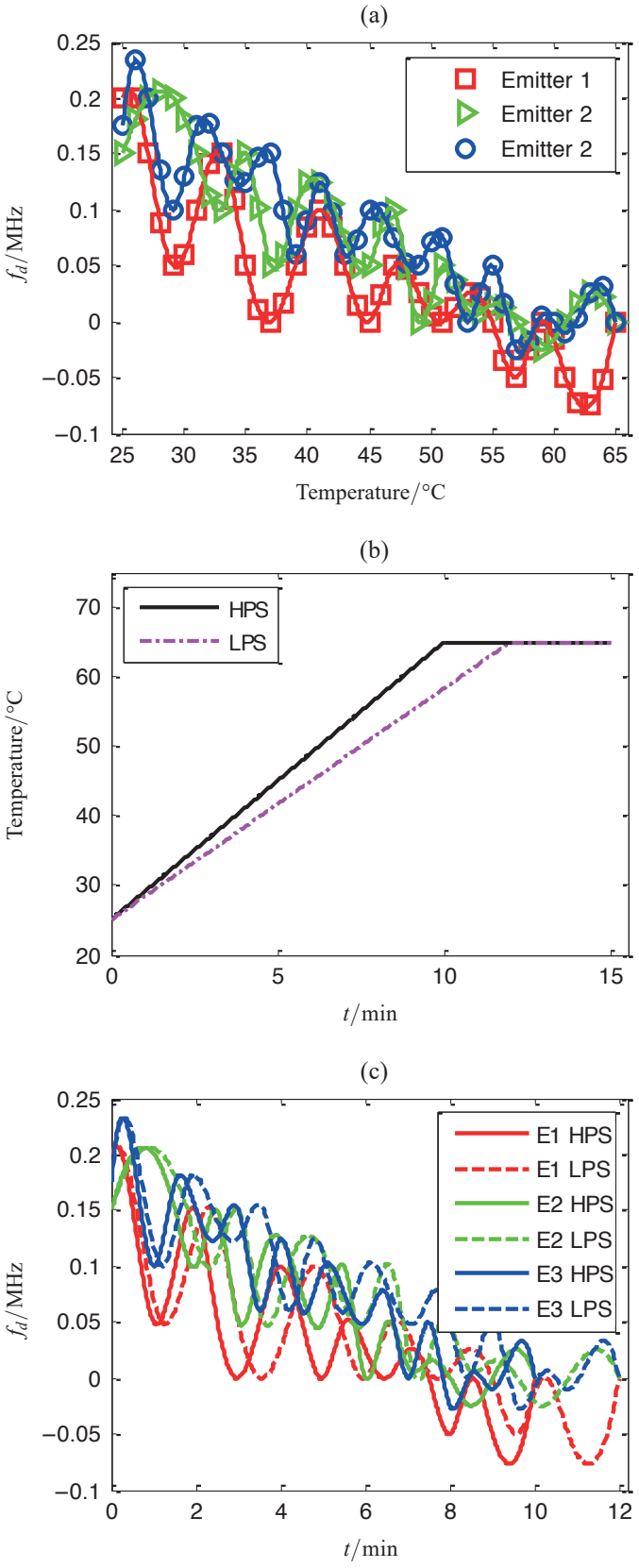

Fig. 2. The relationship among frequency drift, temperature, and time, (a) curves of frequency drift with temperature changes of three emitters, (b) emitters' temperature changes over time under two different start-up power conditions, (c) frequency drift curves of emitter 1, 2 and 3 with two different start-up powers

To develop an algorithm of specific emitter identification using the unintentional modulation features of frequency drift curve, the three problems to be solved are:

- instantaneous frequency estimation process adapted to multicomponent interference is needed;
- FD-curve stretches in the dimension of time in different start-up power conditions, which the feature extraction process and recognition process should be insensitive to;
- the start-up process of an emitter is not fully covered by the observation time window, which causes the incompleteness of an FD-curve.

The algorithm developed in this paper is mainly focused on the first two problems, and the second one is discussed in the most important part of this paper.

3. The proposed algorithm

The process flow of the algorithm proposed in this paper is shown in Fig. 3, which shows instantaneous frequency estimation, FD-curve feature extraction and a recognition process based on support vector machine.

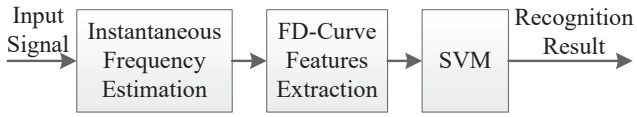

Fig. 3. Process flow of the proposed SEI using FD-curve features

3.1. Instantaneous frequency estimation process. The instantaneous frequency estimation process used in this paper is mainly inspired by the impressive work of Nabeel Ali Khan and Boualem Boashash [25]. The algorithm proposed in [25] is a multicomponent analysis method using time-frequency distributions based on the adaptive fractional spectrogram.

The adaptive fractional spectrogram is developed from the short time Fourier transform, which is defined as

$$\mathrm{STFT}_{\alpha,\sigma}(t,f) = \int s(\tau) h_{\alpha,\sigma}(\tau - t) e^{-j2\pi f\tau} d\tau, \tag{2}$$

where $h_{\alpha,\sigma}(\tau)$ is a Gaussian window expressed as , which has two adaptive parameters, the standard deviation of the Gaussian window σ and the rotation order of a fractional Fourier transform α.

$$h_{\alpha,\sigma}(\tau) = \frac{e^{j\frac{\alpha}{2}}}{\sqrt{j\sin\alpha}} \int_{-\infty}^{\infty} e^{j\pi \frac{(u^2+\tau^2)\cos\alpha - 2\tau u}{\sin\alpha} - \frac{u^2}{2\sigma^2}} du \tag{3}$$

The adaptive fractional spectrogram is finally defined as

$$\mathrm{AFS}(t,f) = \max_{\alpha_{t,f},\,\sigma_{t,f}} \left[\left| \int s(\tau) h_{\alpha_{t,f},\,\sigma_{t,f}}(\tau - t) e^{-j2\pi f\tau} d\tau \right|^2 \right] \tag{4}$$

More detailed information about the instantaneous frequency estimation algorithm can be found in [25–27].

Every frequency drift curve needs a long observing time window of tens of minutes to process. An observing time window consists of many compact time slices. Over a period of observing time, a receiver receives several pulses of the emitting signal in every time slice. During every time slice, the receiver extracts time-frequency distribution of every pulse and gets the instantaneous frequency of the pulse with the method based on adaptive fractional spectrogram. At the same time, the receiver separates all the pulses into different type emitters. During an observing time window, the receiver combines all the pulse instantaneous frequency of every same type emitter successively from every time slice. Finally, the receiver obtains all the specific frequencies of every emitter during the observing time window and connects the specific frequencies into a curve.

3.2. Feature extraction process of an FD-curve. For different emitters, due to incomplete consistency of physical device, their FD-curves are physically different and with different stretching features. But for the same emitter operated with different powers, different stretched FD-curves in time dimension of frequency drift can be observed, which should be classified into the same emitter. Through the proposed feature extraction method of an FD-curve, the receiver can identify the different stretched characteristic curves of frequency shift caused by different start-up powers as the same emitter with particularly defined features, which means the proposed feature extraction method is insensitive to time dimensional stretching. Hence the principle of the feature extraction algorithm of an FD-curve proposed in this paper.

The basic feature extraction idea of an FD-curve is to find the characteristic points to represent the FD-curve. This paper aims to find some characteristic points according to specific rules of an FD-curve to decompose and represent the curve. First, authors attempt to find a specific point to divide the curve into two sub-curves, and then look for another feature points on the divided curves to divide the sub-curves again. After repeating the division several times, a group of feature points on an FD-curve can be obtained and used to represent the curve [28, 29]. Finally, a feature vector defined from the group of feature points can be obtained, and used to identify different emitters.

For example, as the curve AB shown in Fig. 4 defines the first splitting point or feature point on the curve AB as point C,

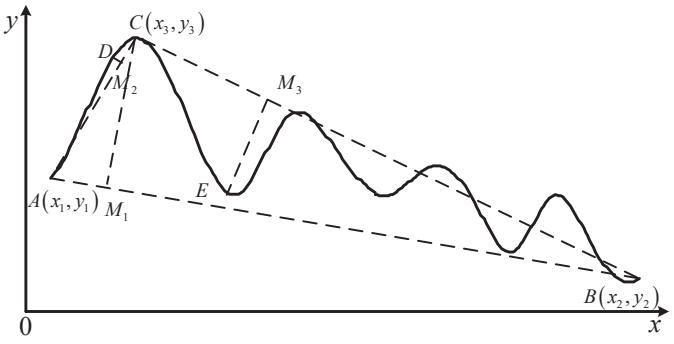

Fig. 4. Feature points extraction of an FD-curve

which has the maximum distance CM_1 from the straight line through point A and point B, called chord AB, and then point C divides the curve AB into sub-curve AC and sub-curve CB, which is the first segmentation shown in Fig. 4. Then point D and point E on the sub-curves of AC and CB are found. They have the maximum distance from chord AC and CB as well, and DM_2 and EM_2 denote corresponding maximum distance, respectively. Point C, point D and point E divide the original curve into sub-curve AD, sub-curve DC, sub-curve CE and sub-curve EB, which is the second segmentation. Then the curve AD, DC, CE and EB is split, respectively, and the points having the farthest distance from the straight line AD, DC, CE and EB on the curve AD, DC, CE and EB are found. The segmentation processing is repeated until the distance from a feature point to its chord is smaller than a specific value. When two or more feature points are found at the same time, the point with the smallest abscissa value is selected as the final feature point.

Define the feature value of a feature point as

$$h = \left| \frac{y_3 + d}{ay_1 + by_2 + d} \right| \tag{5}$$

where a, b, and d is constants. h is defined as the characteristic distance ratio.

The characteristic distance ratio defined by equation (5) is only related to the ordinate value of the endpoints and the feature point, so it is possible that the characteristic distance ratio is insensitive to the FD-curve stretching in time dimension. If the feature point C is also constant no matter how the FD-curve stretches in time dimension, the defined characteristic distance ratio is completely stable for the recognition algorithm.

To prove that the feature point is always constant no matter how the FD-curve stretches in time dimension, is to prove that the feature point still has the maximum distance after stretching.

Point A and point B denote the two endpoints of an FD-curve, point C on the curve has the maximum distance from the straight line AB, which is recorded as CM and shown in Fig. 5. The length of CM according to the formula of distance from point to the straight line is

$$|CM| = \sqrt{|\overrightarrow{AC}|^2 - \left| \frac{\overrightarrow{AC} \cdot \overrightarrow{AB}}{|\overrightarrow{AB}|} \right|^2}. \tag{6}$$

Substituting the coordinate values, the length of CM can be simplified as

$$|CM| = \frac{|x_2 y - x_2 y_1 - x_1 y - x y_2 + x y_1 + x_1 y_2|}{\sqrt{(x_2 - x_1)^2 + (y_2 - y_1)^2}}. \tag{7}$$

If the FD-curve is stretched by a factor m, point A, B and C are transferred to the new point A', B' and C' as shown in

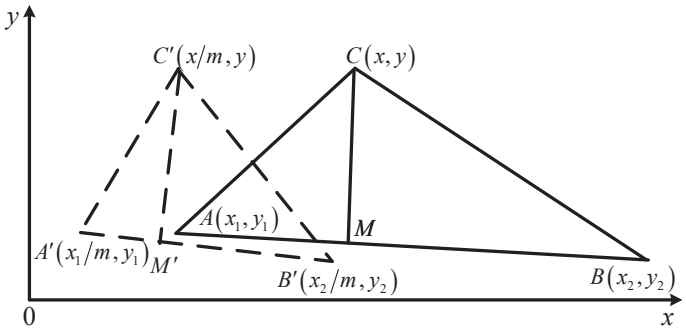

Fig. 5. The endpoints and feature point with horizontal stretching

Fig. 5. The problem is transformed into whether point C' has the farthest distance to the straight line $A'B'$. The distance from point C' to the straight line $A'B'$ is

$$|C'M'| = \frac{\frac{1}{m}|x_2 y - x_2 y_1 - x_1 y - x y_2 + x y_1 + x_1 y_2|}{\sqrt{(x_2 - x_1)^2 + (y_2 - y_1)^2}}. \tag{8}$$

The denominator of the distance expression of any point on the FD-curve to straight line is the same as the denominator of (8), so the distance is the biggest one as long as the numerator is the biggest one. The numerator of equation (8) is almost the same as equation (7) except the stretching factor m. It is easy to see that C' is the new feature point to make the distance $|C'M'|$ the biggest when the previous feature point C makes the length of CM the biggest.

That is to say, the feature point in the new FD-curve keeps the same position relatively after a horizontal stretching. Due to the characteristic distance ratio defined by (5), only related to the ordinate value and the ordinate value of the feature point which remains the same after stretching, the characteristic distance ratio remains constant whether the FD-curve is stretched or not. So the defined characteristic distance ratio is completely insensitive to the FD-curve stretching in time dimension.

The defined characteristic distance ratio, insensitive to the FD-curve stretching in time dimension, makes it possible to be used for specific emitter identification. If an emitter starts up with a different power, the characteristic distance ratio of the feature points extracted from the FD-curve remains the same. In contrast, the characteristic distance ratio of the feature points extracted from different emitters' FD-curves is originally different because the emitters are physically different. Those properties make it perfect for specific emitter identification using the unintentional modulation characteristics of frequency drift curve.

The procedure of the proposed algorithm for feature extraction of an FD-curve is the following.

1) Mark the two end points of an FD-curve AB as the initial left and right end points P and Q, the abscissa of initial end

points are denoted as p and q. Segmentation times k is initially assigned by 1, the number of sub-FD-curve is denoted as i, initially assign the value of constants a, b and d.

2) Find the feature point O on the FD-curve PQ, which has the maximum distance to the straight line PQ. If there is more than one feature point at the same time, select the leftmost point which has the smallest abscissa value, and the abscissa is denoted as o. Then the FD-curve PQ is divided into two sub-curves by the feature point O, and the characteristic distance ratio determined by the point O is

$$h_{ki} = \left| \frac{y(o) + d}{ay(p) + by(q) + d} \right| \tag{9}$$

where $y(g)$is the specific frequency series.

3) Split the FD-curve AB for the k-th time, and $2^k - 1$ feature points can be obtained in the 2^k sub-FD-curves. In the k-th segmentation, a feature sub-vector $\mathbf{h}_k = \left(h_{k,1}, h_{k,2}, \mathrm{L}, h_{k,2^{k-1}}\right)^{\mathrm{T}}$ can be obtained. In the sub-FD-curve of i $\left(i = 1, 2, \ldots, 2^k\right)$, mark the two end points of each sub-FD-curve as the initial left and right end points P and Q, and then execute step 2 processing. Finally, the selected feature points of the k-th segmentation split the FD-curve into 2^{k+1} sub-FD-curves;

4) $k = k + 1$, repeat Step 3 until the characteristic distance ratio is less than a preset threshold or the segmentation times reache a preset threshold.

5) Compose all the characteristic distance ratio into a feature vector for the final recognition, noted as $\mathbf{v} = [\mathbf{h}_1, \mathrm{L}, \mathbf{h}_k]$.

Finally, a specific feature vector can be obtained by the proposed feature extraction process.

The parameters a, b and d in (9) are designed to optimize the feature vector based on Fisher's discriminant ratio (FDR) rule, and the FDR is defined as (10).

$$FDR^{(ij)}(a, b, d) = \frac{\sum\limits_{l=i,j} p^{(l)} \left[\mathrm{E}\left(\mathbf{v}^{(i)}\right) - \mathrm{E}\left(\mathbf{v}^{(j)}\right) \right]^2}{\sum\limits_{l=i,j} p^{(l)} \mathrm{D}\left(\mathbf{v}^{(l)}\right)}, \tag{10}$$

where l is the label of emitter, i and j is the class index number, p is the probability of different emitters, function E denotes the expectation and function D denotes the variance. The probabilities of different emitters are assumed to be the same.

The values of a, b and d can be found by solving the optimization problem

$$\begin{aligned} &\max FDR^{(ij)}(a, b, d), \quad i \neq j \\ &\text{s.t.} \quad 0 \leq a, b \leq 1, 0 \leq d \leq \max(y) \end{aligned} \tag{11}$$

which is an important further topic in the future and is not discussed in this paper. The values used in this paper are empirical, and they are given in the simulation section.

3.3. Recognition process. The recognition technique used in this paper is support vector machine (SVM), which is a machine intelligence algorithm based on the statistical learning theory [30].

The classification function (decision function) for linear separable data is defined as

$$f(x) = \sum_{i=1}^{l} l_i \alpha_i \langle x_i, x \rangle + b \tag{12}$$

where α_i is the Lagrange multiplier, which is always positive, $\langle \cdot, \cdot \rangle$ represents the inner product, $b/\|\mathbf{w}\|$ is the perpendicular distance from the hyperplane to the origin with $\mathbf{w}$ included in $\sum_{i=1}^{l} y_i \alpha_i \langle x_i, x \rangle$, and $\|\cdot\|$ denotes the Euclidean norm. The classification function for nonlinear separable data is defined as

$$f(x) = \sum_{i=1}^{l} l_i \alpha_i K(x_i, x) + b \tag{13}$$

where $K(x_i, x)$ is the kernel function to transform a nonlinear separable problem to a linear separable problem.

For $l = 2$, l_i is always assigned with $\{-1, 1\}$ and (12) or (13) can be rewritten as

$$\hat{f}(x) = \mathrm{sgn}\left[f(x)\right], \tag{14}$$

where sgn is the signum function.

More detailed information about the SVM recognition algorithm can be found in [30]. The SVM used in this paper is a multiclass SVM. The training and identification procedures of the recognition process are the following.

Training procedure:

1) Modulate the emitter signal $s(t)$ using (1) with frequency drift values one by one indicated in Fig. 2(c), which means one point value in in Fig. 2(c) is for one independent signal pulse and one FD-curve is for one group of pulses. So a group of modulated pulses is a sample of an emitter. Let n be the number of samples of an FD-curve and the total amount of samples is N, so N is $6n$ in this paper.
2) Calculate the instantaneous frequency of every pulse using AFS and connect all the specific frequencies of each emitter in each group of pulses into a curve.
3) Extract the feature vector $\mathbf{v}$ of each FD-curve using the feature extraction process presented in Section 3.2.
4) Set the training percentage, denoted as β, and let $\{\mathbf{v}_i, l_i\}$, $i = 1, \ldots, \beta NN$, be the set of training data with $l_i \in \{1, \mathrm{L}, E\}$ as the label of each class and input the training data set into the SVM classifier for training. E is the number of emitters. Then the optimized α_i, $i = 1, \mathrm{L}, E$, and b is obtained.

Identification procedure:

5) Classify the test data denoted as $\{\mathbf{v}_i\}$, $i = 1, \ldots, (1 - \beta)N$, using the trained SVM classifier.
6) For $E = 2$, $\mathbf{v}_i$ is labelled as 1 if $f(\mathbf{v}_i) < 0$, otherwise it is labelled as 2; For $E > 2$, the decision function cannot obtain the result directly. A one-versus-one technique and a max-win voting mechanism are applied. The class winning the most votes is considered as the identification result.

4. Simulation results and analysis

The simulation is organized by obtaining the curve with frequency drift, extracting curve feature vectors and recognition of the emitters.

4.1. Obtaining the curves with frequency drift. Let us make linear frequency modulated (LFM) radars an example of emitters, and the pure signal can be written as

$$s(t) = A\exp\left(j\left(2\pi\left(f_0 t + 0.5kt^2\right)\right)\right) \tag{15}$$

where the amplitude A is 1, the initial frequency f_0 is 22 MHz, the chirp rate k is 0.04 MHz per microsecond, the chirp period and the pulse width are the same, which is 100 μs. So the signal frequency is modulated from 22 MHz to 26 MHz, which means the signal bandwidth is 4 MHz.

Modulate the chip signal with the different frequency drift shown in Fig. 2(c) and transmit the signals through a channel with additive white Gaussian noise. The receiver receives several continuous pulses in every time slice and process the pulses using the proposed algorithm.

Then the received signal can be written as

$$r(t) = s_{fd}(t) + n(t), \tag{16}$$

where $n(t)$ is the Gaussian white noise.

Define the middle frequency of the chirp signal as the instantaneous frequency and calculate the instantaneous frequency of the continuous received pulses with the instantaneous frequency estimation process. Calculate the average instantaneous frequency of the several received signal pulses as the stable frequency in a time slice and connect the stable frequencies between time slices into an FD-curve.

When the signal to noise ratio (SNR) is 0 dB, the obtained FD-curves with frequency drift are presented in Fig. 6. As the error range of frequency measurement is much smaller than the frequency drift range, the FD-curves can easily be extracted automatically by detecting the frequency varying range.

The results shown in Fig. 6 indicate that the empirical results of frequency do not differ much from the theoretical values within an acceptable range, proving that the proposed instantaneous frequency estimation process based on the adaptive fractional spectrogram method is quite effective in the analysis of time-frequency distribution. In Fig. 6, the empirical FD-curves is the results of computer simulation experiments, and the theoretical FD-curves is the same as the emitters in Fig. 2(c), which are regarded as theoretical values.

4.2. Extracting FD-curve feature vectors. Analyze the curves with frequency drift of three emitters working at higher powers and lower powers by the specific feature extraction algorithm of curve in the condition of Gaussian white noise of 0 dB, set a, b and d as 0.5, 0.2 and 0 respectively in (5); let the preset

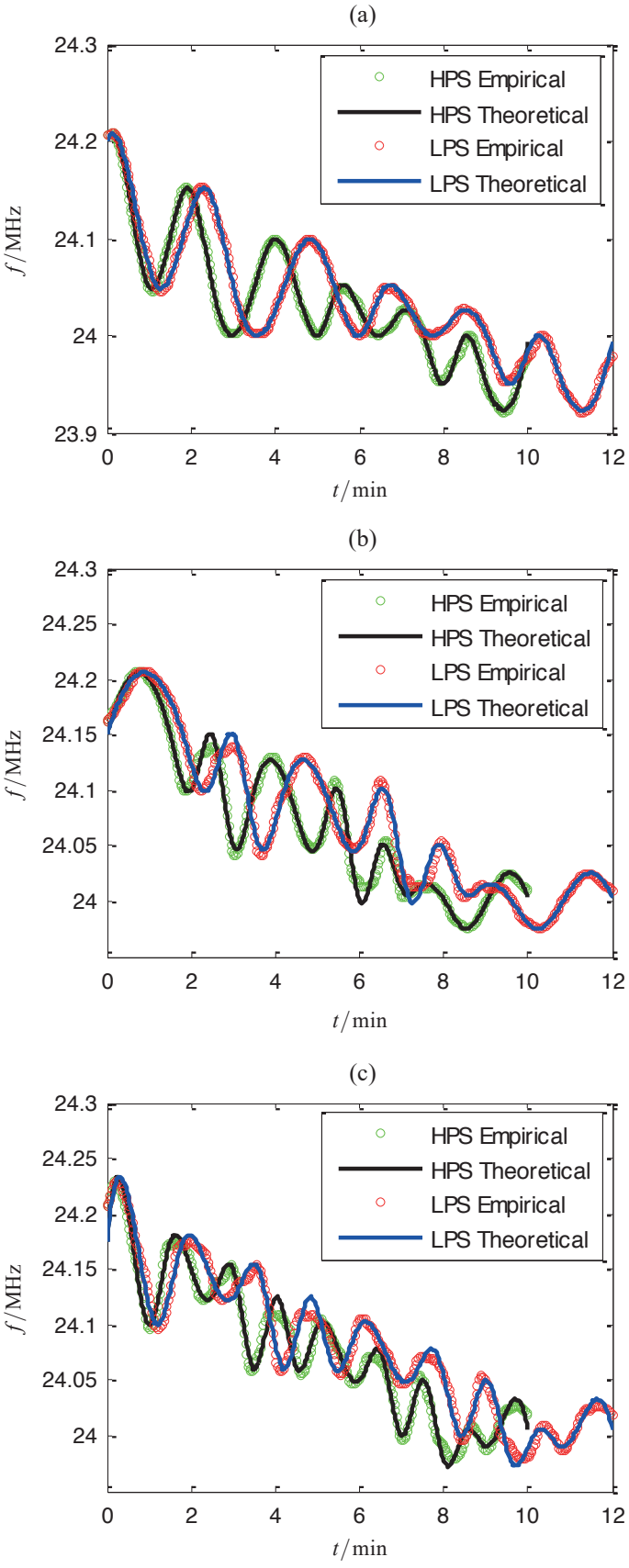

Fig. 6. The FD-curves to be identified when SNR = 0 dB, (a) results of the FD-curve of emitter 1, (b) results of the FD-curve of emitter 2, (c) results of the FD-curve of emitter 3

threshold of the segmentation times be 5. Then the feature vectors of fifteen elements can be obtained for recognition. The fifteen feature elements of the emitters' respective FD-curves are shown in Table 1.

Table 1
Empirical characteristics of the FD-curves of emitters 1, 2, and 3 with two different start-up powers

Feature number	Emitter 1		Emitter 2		Emitter 3	
	HPS	*LPS*	*HPS*	*LPS*	*HPS*	*LPS*
1	1.4204	1.4204	1.4240	1.4240	1.4252	1.4253
2	1.4226	1.4227	1.4294	1.4332	1.4314	1.4315
3	1.4347	1.4347	1.4345	1.4344	1.4346	1.4346
4	1.4307	1.4306	1.4316	1.4303	1.4295	1.4296
5	1.4272	1.4272	1.4300	1.4299	1.4316	1.4314
6	1.4356	1.4355	1.4293	1.4273	1.4295	1.4295
7	1.4248	1.4248	1.4237	1.4237	1.4244	1.4244
8	1.4289	1.4289	1.4303	1.4293	1.4286	1.4286
9	1.4285	1.4285	1.4286	1.4286	1.4283	1.4283
10	1.4272	1.4272	1.4287	1.4236	1.4279	1.4279
11	1.4290	1.4290	1.4292	1.4292	1.4290	1.4291
12	1.4267	1.4267	1.4234	1.4287	1.4287	1.4288
13	1.4319	1.4317	1.4299	1.4299	1.4287	1.4287
14	1.4237	1.4237	1.4256	1.4251	1.4246	1.4246
15	1.4242	1.4242	1.4312	1.4310	1.4321	1.4321

The feature elements shown in Table 1 show that the feature vectors of the same emitter with different startup powers is almost the same, which proves the anti-*t*-flexibility ability of the proposed feature extraction process of an FD-curve.

4.3. Recognition of the emitters. In the recognition experiment of the three emitters, the SNR is set from 0 dB down to –7 dB and other parameters stay unchanged. Each simulation is repeated 1000 times in each SNR condition. Calculate the feature vectors of the FD-curves extracted from three different emitters of the same type working with two different powers. A sample group of 1000 feature vectors for each emitter with each start-up power is obtained in each SNR condition, respectively. Then this paper processes the recognition by support vector machine with the first 20% samples for training and the remaining samples for testing. The recognition results are shown in Fig. 7.

In Fig. 7, the feature number is the number of elements used for emitter identification. For example, if the feature number is 5, then the corresponding identification rate in the abscissa value 5 is the result of the identification rate only using the

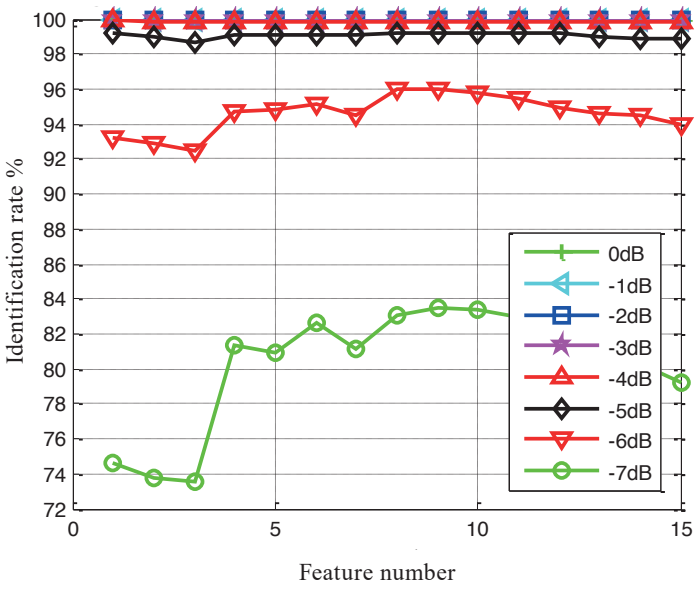

Fig. 7. Results of the specific emitter identification

first 5 elements of the feature vectors. Figure 7 shows that the identification rate generally increases as the feature number increases or the SNR increases. For the frequency drift models built in this paper, the feature number 4 or 5 is appropriate enough for identification, which means the performance of the proposed algorithm is excellent. There are mainly two reasons: firstly, the defined feature can directly and efficiently reflect the geometric signatures of different emitters' FD-curves; secondly, the emitter frequency drift models' individual difference is apparent enough. Predictably the feature number needed for identification increases as the signal frequency drift models' individual difference decreases, and the computation needed for identification processing increases at the same time, which means the proposed algorithm is flexible.

The results in Fig. 7 show that the identification rate is generally more than 98% above –5 dB of SNR, which is excellent enough for most applications. The proposed algorithm is novel; the time length level in Fig. 1 the proposed algorithm focuses on is different from other references, which is a novel view of electronic emitters, so it is inaccurate and unpractical to compare with other algorithms. The identification performance shows that the proposed algorithm is valuable.

5. Real data verification

To verify the performance and practicality of the proposed algorithm, this paper samples the emitted signals from two real devices. One of them is an E4438C made by Agilent, which has been used for more than 10 years and has some significant unintentional modulation features; another one is a radar simulator, which has been used for about 3 years and has weaker unintentional modulation features. To suppress the additional unintentional modulation from the sampling equipment, this

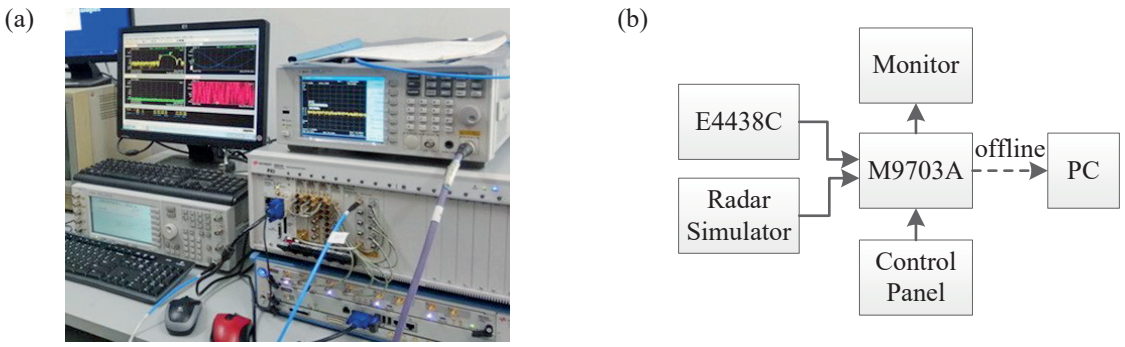

Fig. 8. Real signal sampling experiment, (a) sampling the E4438C, (b) signal sampling and signal processing diagram

paper uses M9703A, which is made by Keysight and has been regulated in less than one year, to sample the signal sources. The real signal sampling experiment is shown in Fig. 8.

After all the measuring instruments are started up and stable, the signal sources are started up with preset configuration. The continues sampling time is about 35 minutes, after which the signal sources are powered off and cooled down with an additional fan in about 25 minutes. The internal Celsius temperature of E4438C varies from about 25 degrees to about 55 degrees and the radar simulator varies from about 25 degrees to about 50 degrees. The temperature increasing rate changes with different signal power output are not obvious enough, which makes the FD-curve stretching in the dimension of time in different start-up power conditions not convenient to be observed. As shown in Fig. 8(b), all the real data is processed offline by another personal computer.

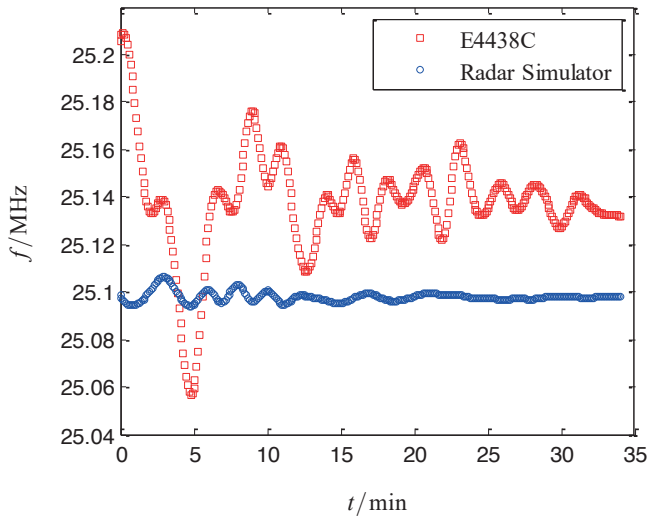

Fig. 9. The FD-curves of E4438C and a radar simulator

The carrier frequency is 425 MHz, the modulation bandwidth is 2 MHz, and thepulse width is 130 μs. The sampling rate is 2 GHz, and the digital down conversion process moves the spectrum to the intermediate frequency 25 MHz. The FD-curves of the two emitters in some start-up process are shown in Fig. 9.

As shown in Fig. 9, the final stable frequencies of the two emitters slightly differ, but the frequency drift curves are obviously different, which proves the years of use affect the unintentional modulation characteristics of an emitter a lot. We have obtained 200 start-up processes of E4438C and the radar simulator each in about a month. The identification rate of the two emitters is 100%, whichprovethe practical performance of the proposed algorithm.

6. Conclusions

In this paper, a geometric method for specific emitter identification is proposed by analyzing the unintentional modulation characteristic of frequency drift. Firstly, frequency drift models based on physical phenomenon are established and the frequency drift parameters are modulated into the pure signal of a typical radar. Secondly, a proposed algorithm for specific emitter identification, consisting of an instantaneous frequency estimation process, a feature extraction process of FD-curves and a recognition process based on SVM, is presented. Finally, the simulation results and analysis are given, and the real data verification proves the practical performance.

As we can see in Fig. 9, the frequency accuracy is relatively higher than general applications. The frequency measurement accuracy is decided by the sampling rate and the sampled signal length. A higher accuracy requires more computation costs and more time. The achieved frequency accuracy in this paper is about 4 kHz. The proposed algorithm with high accuracy can be applied in ELINT systems, information forensics and security systems, etc., where computation resources are relatively abundant. The identification performance of the proposed algorithm is excellent enough for most applications, which is generally more than 98% above –5 dB of SNR. The contribution of the excellent performance is mainly from the accurate instantaneous frequency estimation process and the effective feature extraction process. Another important advantage of the proposed algorithm is its flexibility: the identification rate can be increased by increasing the frequency estimation accuracy and increasing the feature number used for identification in the

cost of increasing computational complexity. Any application can find a balance between identification performance and computational complexity.

Acknowledgements. This paper is supported by the Research Fund of China Aerospace Science and Technology Corporation and the National Natural Science Foundation of China, China [Grant number: 61671185]. The authors also thank the anonymous reviewers for their valuable comments.

References

[1] L.E. Langley, "Specific emitter identification (SEI) and classical parameter fusion technology", in *WESCON/'93. Conference Record*, 1993, 377–381.

[2] K.I. Talbot, P.R. Duley, and M.H. Hyatt, "Specific emitter identification and verification", *Technology Review Journal,* pp. 113–133, 2003.

[3] M.-W. Liu and J.F. Doherty, "Nonlinearity estimation for specific emitter identification in multipath channels", *IEEE Transactions on Information Forensics and Security* 6, 1076–1085 (2011).

[4] A. Kawalec and R. Owczarek, "Specific emitter identification using intrapulse data", in *Radar Conference, 2004. EURAD. First European*, 249–252 (2004).

[5] J. Matuszewski, "Specific emitter identification", *International Radar Symposium*, 1–4 (2008).

[6] A.G. Stove, A.L. Hume, and C.J. Baker, "Low probability of intercept radar strategies", *IEE Proceedings – Radar, Sonar and Navigation* 151, 249 (2004).

[7] V. Krishnamurthy, "Emission management for low probability intercept sensors in network centric warfare", *IEEE Transactions on Aerospace and Electronic Systems* 41, 133–152 (2005).

[8] K.-W. Lee and W.-K. Lee, "The low probability of intercept RADAR waveform based on random phase and code rate transition for Doppler tolerance improvement", *The Journal of Korean Institute of Electromagnetic Engineering and Science* 26, 999–1011 (2015).

[9] J. Dudczyk and A. Kawalec, "Specific emitter identification based on graphical representation of the distribution of radar signal parameters", *Bull. Pol. Ac.: Tech* 63(2), 391–396, (2015).

[10] H. Ye, Z. Liu, and W. Jiang, "Comparison of unintentional frequency and phase modulation features for specific emitter identification", *Electronics Letters* 48, 875–876, (2012).

[11] J. Zhang, F. Wang, O.A. Dobre, and Z. Zhong, "Specific emitter identification via Hilbert-Huang transform in single-hop and relaying scenarios", *IEEE Transactions on Information Forensics and Security* 11, 1192–1205 (2016).

[12] Y. Yuan, Z. Huang, H. Wu, and X. Wang, "Specific emitter identification based on Hilbert-Huang transform-based time-frequency-energy distribution features", *IET Communications* 8, 2404–2412 (2014).

[13] A. Kawalec, R. Owczarek, and J. Dudczyk, "Data modeling and simulation applied to radar signal recognition", *Molecular and Quantum Acoustics* 26, 165–173 (2005).

[14] R. Samborski and M. Ziolko, "Speaker localization in conferencing systems employing phase features and wavelet transform", *2013 IEEE International Symposium on Signal Processing and Information Technology (IEEE Isspit 2013),* 333–337 (2013).

[15] H. Jiang, W. Guan, and L. Ai, "Specific radar emitter identification based on a digital channelized receiver", *5th International Congress on Image and Signal Processing (Cisp),* 1855–1860, (2012).

[16] Z. Tang and S. Li, "Steady signal-based fractal method of specific communications emitter sources identification", in *Wireless Communications, Networking and Applications, Wcna 2014*. vol. 348, eds. Q.A. Zeng, 809–819 (2016).

[17] G. Huang, Y. Yuan, X. Wang, and Z. Huang, "Specific emitter identification based on nonlinear dynamical characteristics", *Canadian Journal of Electrical and Computer Engineering-Revue Canadienne De Genie Electrique Et Informatique* 39, 34–41, (2016).

[18] J. Dudczyk and A. Kawalec, "Identification of emitter sources in the aspect of their fractal features", *Bull. Pol. Ac.: Tech* 61(3), 623–628, (2013).

[19] J. Dudczyk and A. Kawalec, "Fast-decision identification algorithm of emission source pattern in database", *Bull. Pol. Ac.: Tech* 63(2), 385–389 (2015).

[20] Y. Shi and H. Ji, "Kernel canonical correlation analysis for specific radar emitter identification", *Electronics Letters* 50, 1318–1319 (2014).

[21] L. Li, H.B. Ji, and L. Jiang, "Quadratic time-frequency analysis and sequential recognition for specific emitter identification", *IET Signal Processing* 5, 568–574 (2011).

[22] A. Aubry, A. Bazzoni, V. Carotenuto, A. De Maio, and P. Failla, "Cumulants-based radar specific emitter identification", in *Information Forensics and Security (WIFS), 2011 IEEE International Workshop on*, 1–6 (2011).

[23] A. Kawalec and R. Owczarek, "Radar emitter recognition using intrapulse data", in *Microwaves, Radar and Wireless Communications, 15th International Conference on*, vol. 2, 435–438 (2004).

[24] I. Tahir, A. Dexter, and R. Carter, "Noise performance of frequency- and phase-locked CW magnetrons operated as current-controlled oscillators", *IEEE Transactions on Electron Devices* 52, 2096–2103 (2005).

[25] N.A. Khan and B. Boashash, "Instantaneous frequency estimation of multicomponent nonstationary signals using multiview time-frequency distributions based on the adaptive fractional spectrogram", *IEEE Signal Processing Letters* 20, 157–160 (2013).

[26] B. Barkat and K. Abed-Meraim, "Algorithms for blind components separation and extraction from the time-frequency distribution of their mixture", *Eurasip Journal on Applied Signal Processing*, 2025–2033 (2004).

[27] C. Capus and K. Brown, "Short-time fractional Fourier methods for the time-frequency representation of chirp signals", *The Journal of the Acoustical Society of America* 113, 3253–3263, (2003).

[28] G.Q. Lu, H.G. Xu, and Y.B. Li, "Line detection based on chain code detection", *2005 IEEE International Conference on Vehicular Electronics and Safety Proceedings,* 98–103, (2005).

[29] H.H. Chi, H.W. Sun, and X.J. Yang, "Curve tracking with improved chain code algorithm", *2009 IEEE International Conference on Mechatronics and Automation, Vols 1–7, Conference Proceedings,* 4333–4338 (2009).

[30] C.J.C. Burges, "A tutorial on support vector machines for pattern recognition", *Data Mining and Knowledge Discovery* 2, 121–167 (1998).